Stable-phase method for hierarchical annealing in the reconstruction of porous media images

DongDong Chen, Qizhi Teng, Xiaohai He,* Zhi Xu, and Zhengji Li
College of Electronics and Information Engineering, Sichuan University, Chengdu 610065, China
(Received 22 July 2013; revised manuscript received 3 November 2013; published 17 January 2014)

In this paper, we introduce a stable-phase approach for hierarchical annealing which addresses the very large computational costs associated with simulated annealing for the reconstruction of large-scale binary porous media images. Our presented method, which uses the two-point correlation function as the morphological descriptor, involves the reconstruction of three-phase and two-phase structures. We consider reconstructing the three-phase structures based on standard annealing and the two-phase structures based on standard and hierarchical annealings. From the result of the two-dimensional (2D) reconstruction, we find that the 2D generation does not fully capture the morphological information of the original image, even though the two-point correlation function of the reconstruction is in excellent agreement with that of the reference image. For the reconstructed three-dimensional (3D) microstructure, we calculate its permeability and compare it to that of the reference 3D microstructure. The result indicates that the reconstructed structure has a lower degree of connectedness than that of the actual sandstone. We also compare the computation time of our presented method to that of the standard annealing, which shows that our presented method of orders of magnitude improves the convergence rate. That is because only a small part of the pixels in the overall hierarchy need to be considered for sampling by the annealer.

DOI: 10.1103/PhysRevE.89.013305 PACS number(s): 95.75.Mn, 05.20.−y, 61.43.−j

I. INTRODUCTION

Porous media, whose microstructures have significant effects on their macroscopic properties (such as mechanical, capillary, electrical conductivity, and permeability), are composed of solid material skeletons and many crowded tiny pores created by the partition of material skeletons [1–9]. To understand how the microstructure of porous media affects their macroscopic properties, one needs the real three-dimensional (3D) structure of porous media. In many cases, only the two-dimensional (2D) structure can be obtained. In this case, the foundation of the researching method is to generate the 3D microstructure of porous media based on the original 2D image. An effective reconstruction procedure enables one to generate accurate structures, and a subsequent analysis can be performed on the 3D structure to obtain the desired macroscopic properties of the media.

The reconstruction procedure can be regarded as an optimization problem, which can be seen as finding a realization (configuration) that makes the discrepancies between the statistical properties of the realization and that of the original 2D structure minimized. Recently, two general approaches [10–22] based on statistical reconstructions have actively been pursued. The first method is based on the conditioning and truncation of Gaussian random fields [10–13]: successively passing a normalized uncorrelated random Gaussian field through a linear and then a nonlinear filter to yield the discrete values representing the phases (or states) of the structure. This approach is mathematically elegant and computationally very efficient but model dependent, so it can only impose the volume fraction and the two-point probability function as constraints for reconstruction. This is a drawback, and even more serious, it is difficult to generalize the structures for systems with more than two phases. Another popular stochastic approach to reconstruct the 3D microstructure of a porous medium is the simulated annealing (SA) reconstruction algorithm [14–21]. This method was first introduced by Rintoul and Torquato in 1997 [22], which starts with a given, arbitrarily chosen, initial configuration of a random medium and a set of target functions. By continuously interchanging the phases of pixels in the digitized system, the target function is gradually coming close to the minimum, which illustrates that the reconstruction has a similar distribution as the experimental structure. This method is model independent and, in principle, it can include any type and number of statistical correlation functions as microstructure information. In addition, it is a global optimization algorithm and can generate the optimum structure making the discrepancies of statistical properties between the generation and the original 2D image minimized.

The attractive convergence property of the SA algorithm [14–22] is offset rapidly by the high demand for computational resources, particularly for the reconstruction of a large-scale microstructure—very common in porous media. To enhance the rate of convergence, several methods were proposed within the SA reconstruction framework. Jiao and co-workers proposed the "surface optimization" rule [14]. In this rule, pixels are grouped into two subsets: low-energy subsets and high-energy subsets. Only the pixels in the high-energy subset are selected. These biased pixel selection rules exclude certain pixels from being selected. Our group proposed a different-phase-neighbor- (DPN-) based pixel selection rule [23]. In this rule, the selection probability of a pixel is determined by the number of its DPNs, which does not exclude any pixel from being selected. These methods, indeed, accelerate the rate of convergence, but they are still very large computational costs for generating the large-scale microstructure.

Another important method for improving the rate of convergence is a hierarchical simulated annealing (HSA) algorithm, which is proposed by Alexander and co-workers [24–26]. In the procedure of hierarchical reconstruction, the larger-scale structures are obtained from coarser scales. Because each scale is treated as a separate annealing procedure, the finer

*Corresponding author: hxh@scu.edu.cn

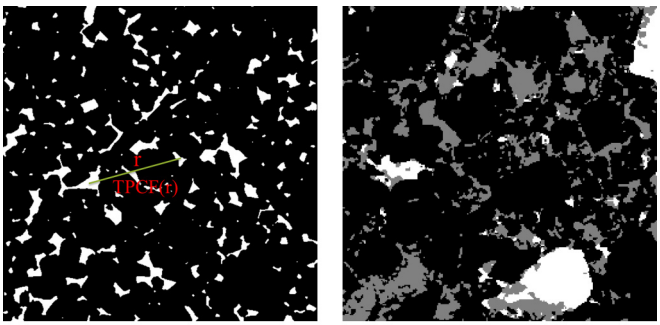

(a) (b)

FIG. 1. (Color online) The microstructure of two random reservoir sandstones. (a) Two-phase microstructure (black, grain; white, void). (b) Three-phase microstructure (black, grain; gray, clay; and white, void).

structure can be eroded or can be destroyed. The more serious drawback is that this method continues to visit every pixel at every scale, including the finest scale, so there remains a substantial computational burden for visiting very large numbers of pixels at the finest scale. In this paper, we propose a truly hierarchical method (the stable-phase method) in which large-scale structures are synthesized and are fixed in place at coarse scales where only local fine-resolution details remain to be refined at finer scales. Because only a small part of the pixels in the overall hierarchy need to be considered for sampling by the annealer, our presented method of orders of magnitude improves the convergence rate and the quality of the final result. The rest of this paper is arranged as follows: The description of the two-point correlation function (TPCF) [27] for the three-phase microstructure is given in Sec. II. In Sec. III, our presented method is briefly outlined. In Sec. IV, the reconstruction of three-phase and two-phase structures based on the original 2D images are performed. For the reconstructed 3D structure, we evaluate its transport property and compare it to that of the real sandstone. Finally, remarks are concluded in Sec. V.

II. REPRESENTATION OF THE TWO-POINT CORRELATION FUNCTION

The date for the TPCF is acquired [27] by throwing numbers of random vectors on the microstructure, determining the likelihood of the beginning and end of each vector ($\vec{r}$) lying in a particular phase and examining the number fraction of the sets (vectors) that satisfy the different phases [Fig. 1(a)]. For a two-phase microstructure, there exist two phases, phase 1 and phase 2, with the volume fraction of each phase defined as follows:

$$\frac{V_k}{V_{\text{total}}} = v_k, \qquad k \in [1,2], \tag{1}$$

where V_1 and V_2 are the volumes of the two phases, respectively, and v_1 and v_2 are their corresponding volume fractions. Clearly,

$$\sum_{k=1}^{2} V_k = V_{\text{tot}} \quad \text{and} \quad \sum_{k-1}^{2} v_k = 1. \tag{2}$$

If the N number of random points is thrown into a given microstructure and the number of points falling into phase k is N_k, then the one-point probability function (P_k) can define the volume fraction through the following relation as N (the total number) is increased to infinity:

$$P_k = \left.\frac{N_k}{N}\right|_{N\to\infty} = v_k. \tag{3}$$

Now, assign a vector starting at each of the random points in a two-phase microstructure as shown in Fig. 1(a). Depending on whether the head and the tail of these vectors fall within phase 1 or phase 2, there will be four different probabilities ($P_{11}, P_{12}, P_{21}, P_{22}$) defined as follows:

$$P_{kl}(\vec{r}) = \left.\frac{N_{kl}}{N}\right|_{N\to\infty} \{\vec{r} = \vec{r}_l - \vec{r}_k, (\vec{r}_l \in \phi_l) \cap (\vec{r}_k \in \phi_k)\}, \tag{4}$$

where N_{kl} is the number of vectors with the head in phase k (ϕ_k) and the tail in phase l (ϕ_l). Equation (4) defines a joint probability distribution function for the occurrence of events constructed by two points as the head and tail of a vector when it is randomly thrown into a microstructure N number of times. The two-point probability function can be defined based on two other probability functions such that

$$P_{kl}(\vec{r}) = P\{(\vec{r}_l \in \phi_l)|(\vec{r}_k \in \phi_k)\} P(\vec{r}_k \in \phi_k). \tag{5}$$

The first term on the right hand side of Eq. (5) is a conditional probability function. Note that, at very long distances $\vec{r} \to \infty$, the probability of occurrence of the head point does not affect the tail point and the two points become uncorrelated or statistically independent and the conditional probability function reduces to a one-point function,

$$P(\vec{r}_k \in \phi_k) = P\{(\vec{r} \to \infty), (\vec{r}_k \in \phi_k)|(\vec{r}_l \in \phi_l)\}. \tag{6}$$

The two-point correlation function will then be reduced to

$$P_{kl}(\vec{r}) = P(\vec{r}_l \in \phi_l) P(\vec{r}_k \in \phi_k), \tag{7}$$

or

$$P_{kl}(\infty) = v_k v_l. \tag{8}$$

For the periodic boundary condition of the microstructure, the two-point correlation function satisfies the following relationship:

$$P_{kl}(\vec{r}) = P_{lk}(\vec{r}). \tag{9}$$

For a three-phase microstructure as shown in Fig. 1(b), the indices (k,l) in the probability function representation extend to three, and as a result, we have nine probabilities ($P_{11}, P_{12}, P_{13}, P_{21}, P_{22}, P_{23}, P_{31}, P_{31}, P_{33}$). Due to normality conditions, the following equations are satisfied:

$$\sum_{k=1-3} \sum_{l=1-3} P_{kl}(\vec{r}) = 1, \tag{10}$$

$$\sum_{l=1-3} P_{kl}(\vec{r}) = v_k, \tag{11}$$

$$\sum_{k=1-3} P_{kl}(\vec{r}) = v_l. \tag{12}$$

Satisfying all three conditions for a three-phase microstructure [k,$l \in (1-3)$] and knowing that the probability functions are

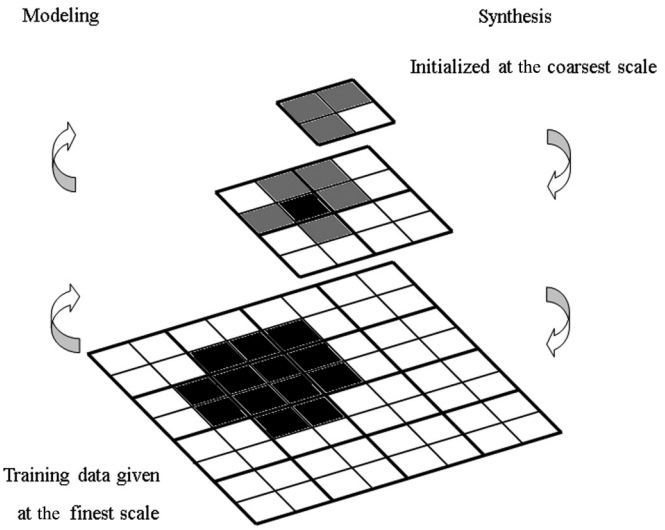

FIG. 2. The rules of modeling and synthesis in hierarchical reconstruction.

symmetric ($P_{kl} = P_{lk}$), three nonlinear correlation equations can be obtained as follows:

$$P_{11} + P_{12} + P_{13} = v_1, \tag{13}$$

$$P_{21} + P_{22} + P_{23} = v_2, \tag{14}$$

$$P_{31} + P_{32} + P_{33} = v_3, \tag{15}$$

and the nine probability functions will be reduced to six independent functions ($P_{11}, P_{12}, P_{13}, P_{22}, P_{23}, P_{33}$), resulting in the important conclusion that only three of the nine probabilities should be considered as independent variables. For instance, P_{11}, P_{12}, and P_{22} can be chosen as the three probability parameters. The other probability functions can be obtained through Eqs. (13)–(15). In all reconstructed systems, we assume isotropy of the evolving system, and the sampling is, therefore, performed only along orthogonal directions. It is observed that this sampling procedure can be more accurate than that by random sampling (throwing random points into the system) because the former exhaustively incorporates information from every pixel in the entire system.

III. HIERARCHICAL SIMULATED ANNEALING ALGORITHM

To solve the problem of slow convergence in simulated annealing [14–22], we introduce a stable three-phase hierarchical annealing. An illustration of the three-phase hierarchy is shown in Fig. 2, which contains two parts: modeling and synthesis. In modeling, let $x^{(s)}$ represent an image at scale s where decreasing s signifies progressively coarser scales, and let $x_i^{(s)}$ denote the pixel value of $x^{(s)}$ at position i; $x_i^{(s)} \in \{0,128,255\}$ (three phases: black, gray, and white). Let $\{i_1, i_2, i_3, i_4\}$ be the indices of the children of $x_i^{(s-1)}$ at scale s. For a given binary, the finest-scale image $x^{(s)}$, the coarser-scale representation $x^{(s-1)}$, can be obtained from modeling using

$$x_i^{(s-1)} = \begin{cases} 0, & \text{if } x_{i_j}^{(s)} = 0 \quad \forall j, \\ 255, & \text{if } x_{i_j}^{(s)} = 255 \quad \forall j, \\ 128, & \text{otherwise.} \end{cases} \tag{16}$$

The repeated use of (16) makes the original high-resolution image coarsened to generate a series of target microstructures for the hierarchical method at each resolution level as illustrated in Fig. 2.

In synthesis, a corresponding set of rules is established as constraints on the annealing,

$$\text{if } x_i^{(s-1)} \in \{0,255\}, \quad \text{then } x_{i_j}^{(s)} = x_i^{(s-1)}, \tag{17a}$$

$$\text{if } x_i^{(s-1)} = 128, \quad \text{then } x_{i_j}^{(s)} = 0, \quad \text{or} \quad x_{i_j}^{(s)} = 128. \tag{17b}$$

The outcome of (17) is that each phase in the sample space visited by the annealer must be consistent under (16) with the result at all coarse scales. Black and white pixels stand for the stable phase in the image domain that is preserved at all finer scales. If the pixel is gray in a coarse scale, then the corresponding set of pixels at finer scales can be black, white, or gray. All pixels satisfied (17a) can be ignored in the annealing sampler because their values previously have been stable.

Figure 2 illustrates the process of this coarsening method. Progressively coarser model information is extracted using expression (16) based on a large binary training image. Synthesis begins with some coarse initialization, and annealing is carried out at progressively finer scales (each scale is treated as a separate annealing procedure), constrained by the results of the previous scale according to (17). When annealing at the final finest-scale result, it is affirmed that all values of the pixels must be 0 or 255.

In the procedure of hierarchical reconstruction [24–26], some energy function $E(x)$ is needed. Numbers of energy models have been proposed where the two-point correlation function is a classic statistical function mainly containing a number of properties of training images. Here the two-point correlation function is chosen as the energy function. Let $P_{ij}^{(s)}$ [$i, j \in (1,2)$ for two phases and $i, j \in (1-3)$ for three phases] express the two-point correlation function of the reference image at scale s. And let $P_{ij}(x^{(s)})$ denote the two-point correlation function of the generation at scale s. In the process of hierarchical reconstruction, the calculation of the energy function is based on the phases of the reference image. If the reference image has two phases, there only needs to be one independent two-point correlation function to reconstruct its corresponding microstructure. If the reference image has three phases, three independent two-point correlation functions are needed as discussed in Sec. II,

$$E(x^{(s)}) = \sum_r \left[P_{11}(x^{(s)}) - P_{11}^{(s)}\right]^2 \text{ for two phases,} \tag{18a}$$

$$E(x^{(s)}) = \sum_r \left[P_{11}(x^{(s)}) - P_{11}^{(s)}\right]^2 + \sum_r \left[P_{12}(x^{(s)}) - P_{12}^{(s)}\right]^2 + \sum_r \left[P_{22}(x^{(s)}) - P_{22}^{(s)}\right] \text{ for three phases.} \tag{18b}$$

To evolve the digitized system toward the reference medium (or in other words, minimizing E), the states of two arbitrarily

selected pixels of different phases are interchanged. After the interchange is performed, we can calculate energy E' of the new state and the energy difference $\Delta E = E' - E$ between two successive states of the system. The new state then is accepted with probability $p(\Delta E)$ via the Metropolis method as

$$p(\Delta E) = \begin{cases} 1, & \Delta E \leqslant 0, \\ \exp\left(-\frac{\Delta E}{T}\right), & \Delta E > 0, \end{cases} \tag{19}$$

where T is the "temperature." The decreased rate of T is controlled by a cooling schedule which controls the system to evolve to the desired state as quickly as possible without falling into any local energy minimum. Because each scale is treated as a separate annealing procedure, the algorithm terminates for each scale when energy E [given by Eq. (18)] is less than some small tolerance value or when the number of consecutive unsuccessful phase interchanges is greater than a large number. In each scale, our presented method is not sensitive to the choice in annealing schedule. That is because the large-scale structures are fixed at coarser scales, and finer scales cannot destroy or cannot erode these structures. For a given scale, only a small subset of pixels is needed to be visited. This makes that much larger domains become computationally tractable.

IV. DISCUSSION AND RESULTS

As stated in Sec. III, the method of hierarchical reconstruction involves the three-phase and two-phase reconstructions. In this section, we first discuss the 2D reconstruction of three-phase structures based on standard annealing. Second, the 2D reconstruction of two-phase structures is performed on standard annealing and hierarchical annealing, respectively. Finally, our presented method is applied to perform a 3D reconstruction of the sandstone sample. For the reconstructed 3D microstructure, we calculate its permeability and compare it to that of the actual sandstone. In the procedure of reconstruction, we set the white phase as phase 1, the gray phase as phase 2, and the black phase as phase 3.

A. The 2D reconstruction of the three-phase structure

As an initial test for the three-phase structure, an interpenetrating disk model is generated, displayed in Fig. 3(a), which is digitized into 256 × 256 pixel arrays. To effectively reconstruct the three-phase structure, three independent two-point probabilities are needed, so we choose the probabilities of P_{11}, P_{12}, and P_{22} as the constraints. The simulation starts from random initial configurations (the randomly generated phase 1, phase 2, and phase 3 with fixed volume fractions $\phi_1 = 0.121$, $\phi_2 = 0.067$, and $\phi_3 = 0.812$). After generating an initial microstructure, two arbitrary pixels of different phases are selected and are interchanged forming a new microstructure. The energy difference between the initial and the new state of the system decides the accepted probability of the new state. After sufficiently being interchanged, the energy difference between the original image and the reconstruction is close to the minimum. The reconstruction result and the reference structure are shown in Fig. 3. Note that, although the correlation functions of the reconstructed structure agree

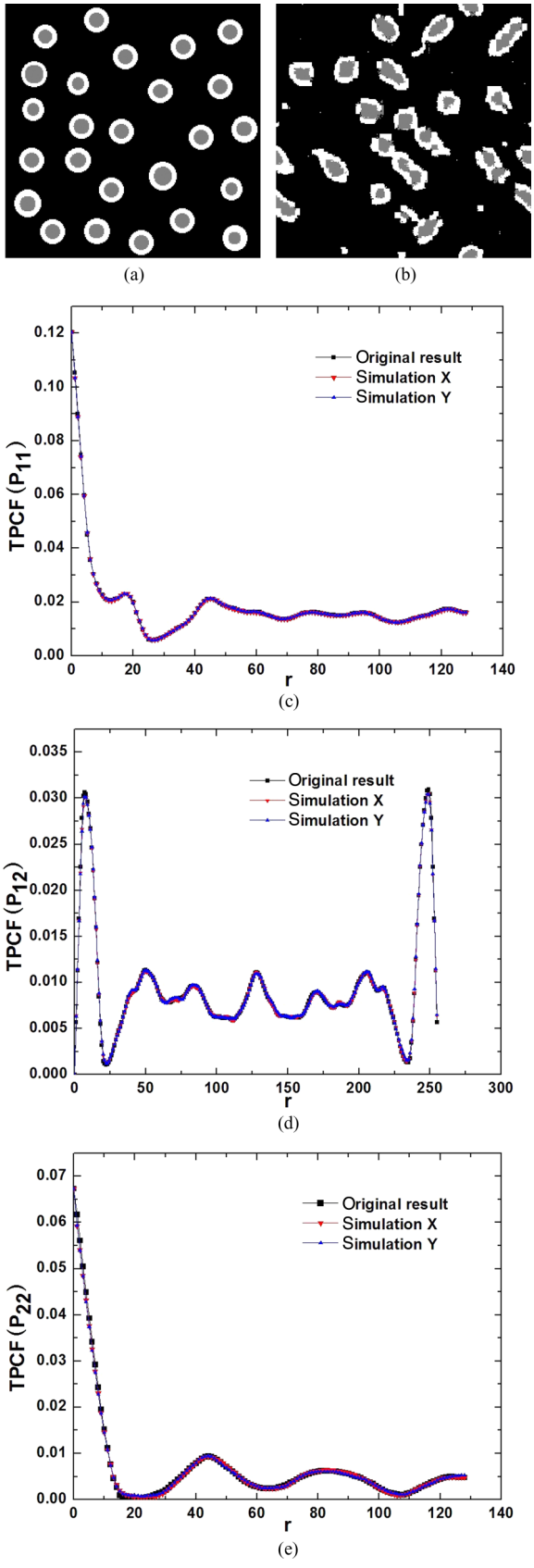

FIG. 3. (Color online) (a) and (b) are the original and the reconstructed three-phase structures, respectively. (c)–(e) are the comparison diagrams of the two-point correlation function for the original and the reconstructed images.

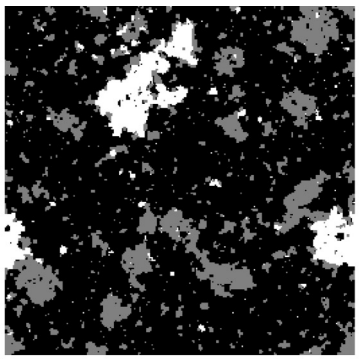

(a)

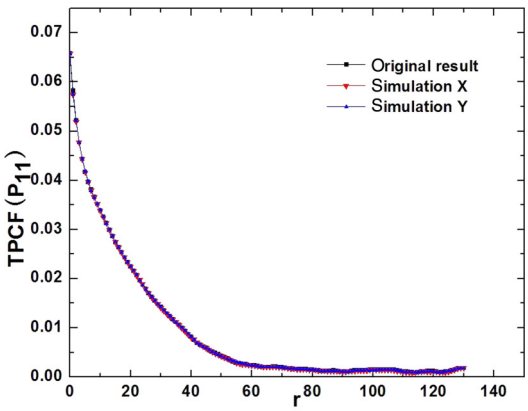

(b)

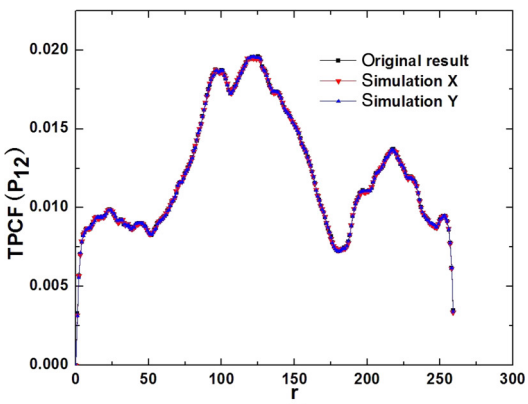

(c)

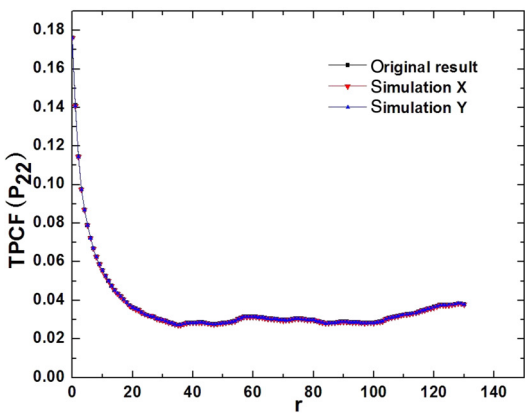

(c)

FIG. 4. (Color online) (a) is the reconstruction of Fig. 1(b). (b)–(d) are the comparisons of the two-point correlation function for the original and the reconstructed images.

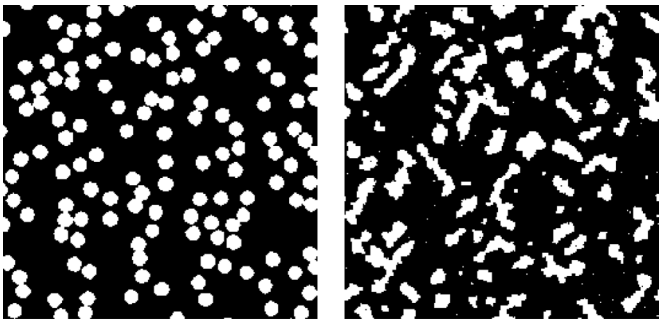

(a) (b)

FIG. 5. (a) and (b) are the original and the reconstructed binary structures, respectively, based on standard annealing.

strikingly well with that of the reference image, the visual images do not appear to be similar. This is because the two-point correlation functions generally do not contain sufficient information to uniquely determine a structure.

Figure 1(b) shows another three-phase microstructure where the phases are defined as: The white color is the void named phase 1, the gray and black colors are the clay named phase 2, and the grain is named phase 3, respectively. And its volume fractions are $\phi_1 = 0.066, \phi_2 = 0.176$, and $\phi_3 = 0.758$. After generating an initial microstructure and interchanging the different phases sufficiently, the reconstructed image shown in Fig. 4(a) has similar morphological information as that of the original image. And the comparisons of the three independent two-point correlation functions between the reconstruction and the real image are plotted in Figs. 4(b)–4(d), respectively. The result shown in Fig. 4 illustrates that the realization of the three-phase microstructure has similar morphological information as the original image and their correlation statistics match fairly well.

B. Standard and hierarchical reconstructions on the binary structure

An equilibrium distribution of binary hard disks shown in Fig. 5(a) will be studied by the standard and hierarchical reconstruction methods. In the standard reconstruction, a random initial structure (the same volume fractions of different phases with that of the original image) is generated first. Then, the different phases of the structure are chosen and are interchanged. After interchanging the different phases sufficiently, the optimum structure is obtained. A realization of the standard reconstruction is shown in Fig. 5(b). In the procedure of hierarchical reconstruction, its corresponding coarser-scale representations are generated first as the reference images, displayed in Figs. 6(a)–6(d). Then, according to the phases of the reference image, different two-point correlation functions are chosen as the energy function: Only one independent two-point correlation function P_{11} is needed for the reconstruction of the two-phase microstructure, and three independent two-point correlation functions of P_{11}, P_{12}, and P_{22} are needed as the energy function for the reconstruction of the three-phase structure. Annealing starts at some coarse initialization structure (32×32) and progressively performs at finer scales (each scale is treated as a separate annealing

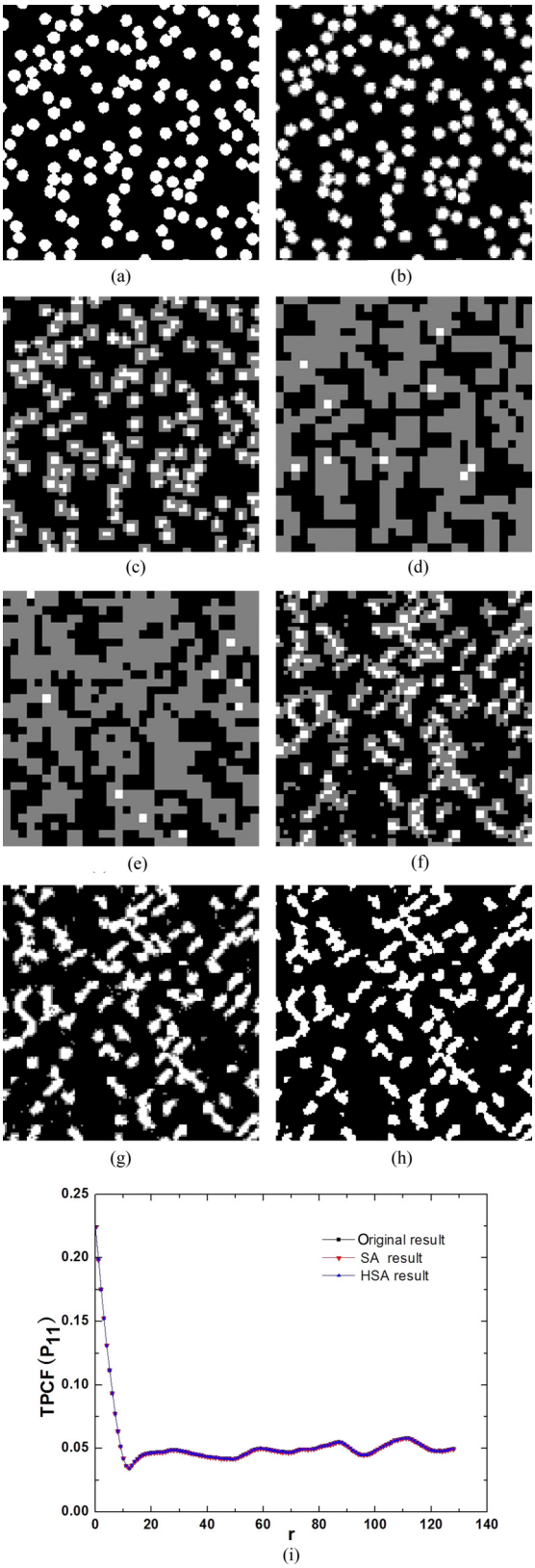

FIG. 6. (Color online) (a) is the original image at a full resolution of 256 × 256. (b) 128 × 128, (c) 64 × 64, and (d) 32 × 32 are its corresponding coarser scales. (e) 32 × 32, (f) 64 × 64, (g) 128 × 128, and (h) 256 × 256 are the results of the hierarchical reconstruction. (i) is the comparison of the two-point correlation function for both the reconstructed structures and the original structure.

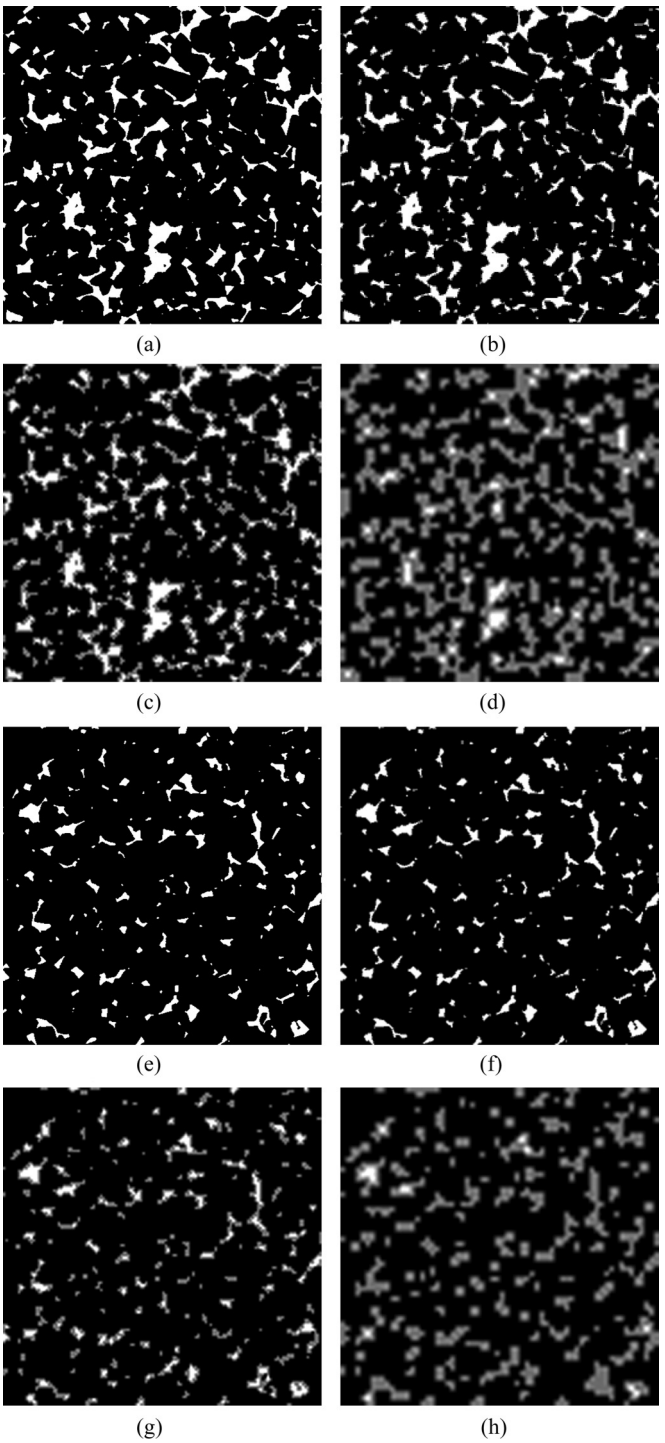

FIG. 7. (a) and (e) are two random reservoir sandstones at full resolutions of 512 × 512. (b) 256 × 256, (c) 128 × 128, (d) 64 × 64, (f) 256 × 256, (g) 128 × 128, and (h) 64 × 64 are their corresponding subsamplings.

procedure), constrained by the result of the previous scale according to (17). All pixels satisfied (17a) are ignored in the annealing sampler as their values have previously been stable. As scale s increased, only a small part of the pixels need to be considered in the annealing sampler. The results of hierarchical reconstruction are shown in Figs. 6(e)–6(h).

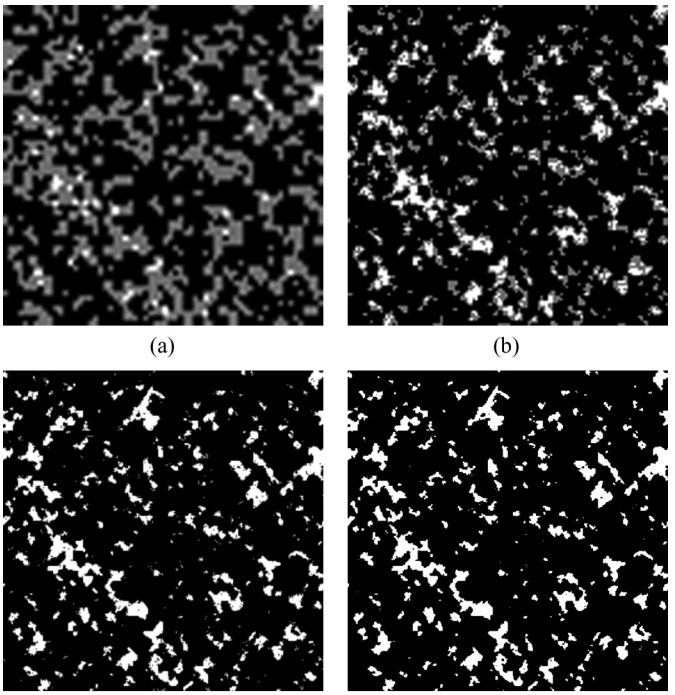

FIG. 8. The results of the hierarchical reconstruction for the image in Fig. 7(a). (a) 64 × 64, (b) 128 × 128, (c) 256 × 256, and (d) 512 × 512.

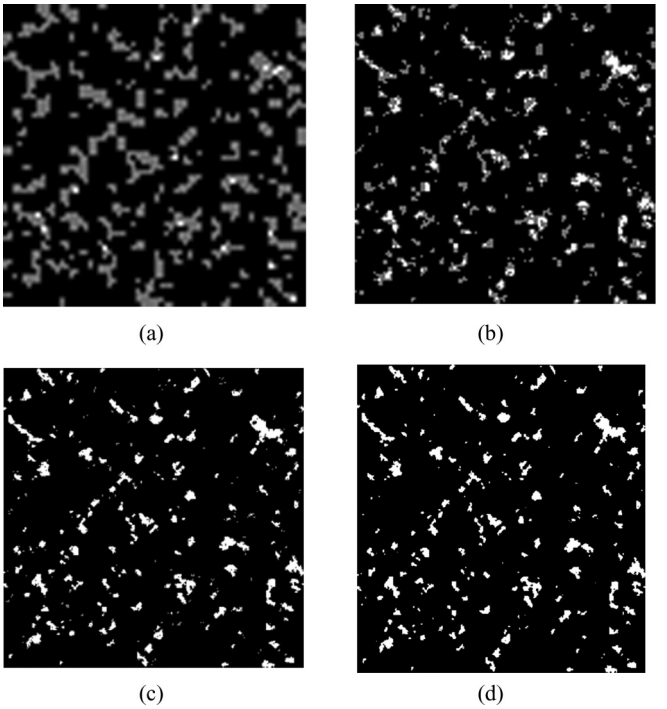

FIG. 9. The results of the hierarchical reconstruction for the image of Fig. 7(e). (a) 64 × 64, (b) 128 × 128, (c) 256 × 256, and (d) 512 × 512.

Note that both reconstructed structures can match the original correlation function very well [displayed in Fig. 6(i)] but yet have a significantly different structure. This nonuniqueness is because the lower-order correlation function generally does not contain complete morphological information.

The hierarchical reconstruction of the real random media is something we are interested in. Two random reservoir sandstone images are chosen, shown in Figs. 7(a) and 7(e). Their corresponding coarser-scale representations are displayed in Figs. 7(b)–7(d) for Fig. 7(a) and Figs. 7(f)–7(h) for Fig. 7(e), respectively. Annealing begins at some coarse initialization structure (64 × 64) and progressively performs at finer scales. The results of the hierarchical reconstruction for Figs. 7(a) and 7(e) are shown in Figs. 8 and 9, respectively. The synthesis results of Figs. 8 and 9 exhibit the similar features observed in the reference images, except that the void regions typically are more rounded in shape. This implies that the hierarchical annealing method can reproduce the salient morphological information of the original image using the two-point correlation functions. And the comparisons of the two-point correlation function between the reconstructions and the real images are plotted in Figs. 10(a) and 10(b), respectively. Note that the realizations based on the method described here have similar morphological information as that of the original images and their correlation statistics are statistically indistinguishable.

C. The reconstruction of the 3D microstructure

The method of hierarchical reconstruction has been performed on two random reservoir sandstone images, and the results illustrate that our presented method can reproduce a similar distribution as the original image. The main aim of our presented method is to solve the high demand for computational resources and to enhance the rate of convergence for the reconstruction of the high-resolution microstructure. In the following, this method is applied to reconstruct the reservoir sandstone at a very high resolution of 256 × 256 × 256 where each of the pixels constitutes a cubic region of size $7.5 \times 7.5 \times 7.5\mu\ \mathrm{m}^3$. For the reconstructed 3D microstructure, we calculate its permeability and compare it to that of the real sandstone.

Figure 11 shows the procedure for the hierarchical reconstruction, which is started at the coarse initialization structure (32 × 32 × 32). In the intermediate scales in Fig. 11, gray pixels, whose values have not yet been stabilized, are present on the interface between black and white regions. The progressive thinning of the gray mediation demonstrates the significance in the reduction in computational complexity since the number of sites sampled at scale s is limited directly by the number of gray pixels presented in the converged result at scale $s - 1$. The number and proportion of the pixels to be visited in a single pass of the annealer as the scale increases from (32 × 32 × 32) to (256 × 256 × 256) for Fig. 11 are plotted in Fig. 12. As seen in Fig. 12(b), the pixels to be visited are normally only a small fraction of the total, especially at fine scales.

The most significant advantage of the presented model is the reduction in the computation time in the process of reconstruction. The comparison of the energy vs computation time between the standard and the hierarchical sampling is shown in Fig. 13(a). It is noted that the energy of the hierarchical annealing drops rapidly and the energy is

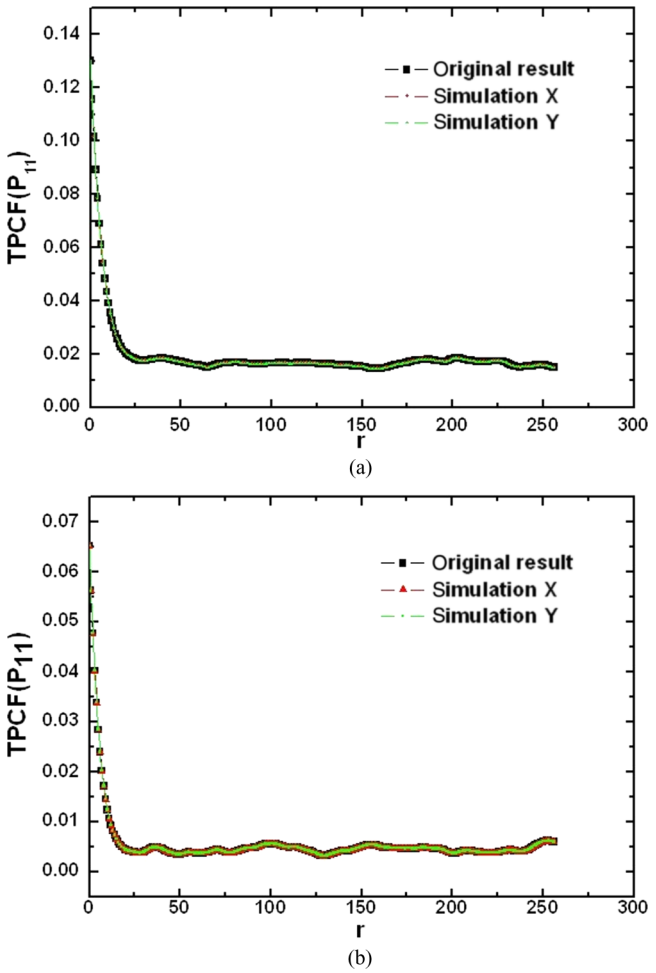

FIG. 10. (Color online) A comparison diagram of the two-point correlation function for the original and the reconstructed images. (a) is the comparison of the two-point correlation function for Figs. 7(a) and 8(d). (b) is the comparison of the two-point correlation function for Figs. 7(e) and 9(d).

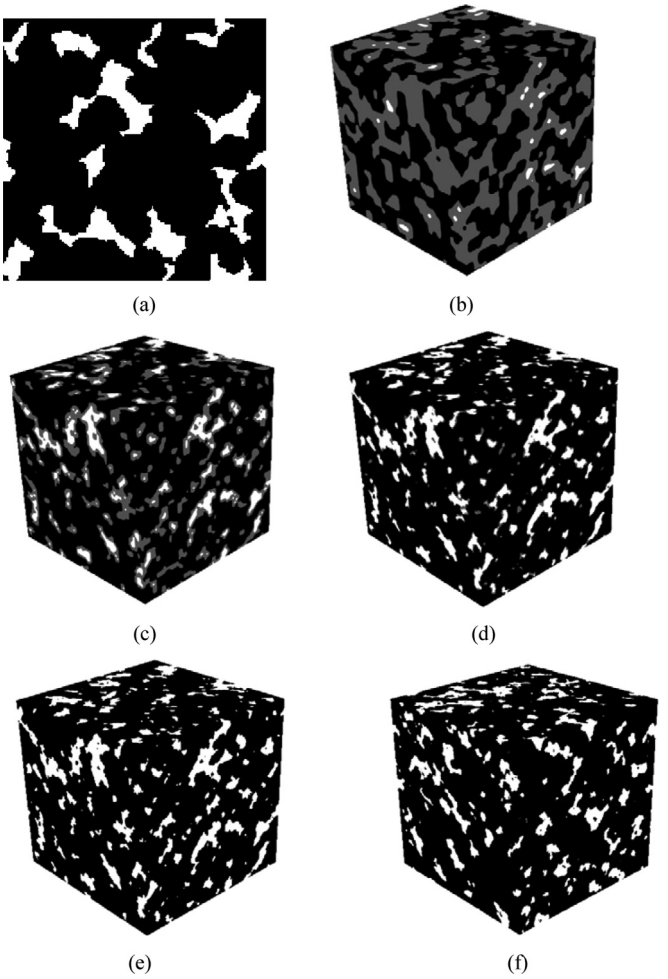

FIG. 11. (a) Training image and the results of the hierarchical reconstruction and the standard reconstruction.(a) Training image at 256 × 256, (b) initial ternary result at 32 × 32 × 32, (c) ternary result at 64 × 64 × 64, (d) ternary result at 128 × 128 × 128, (e) final result at 256 × 256 × 256, and (f) binary result. The unstable regions are represented in gray.

converged very low compared with that of the standard annealing. The energy "spikes" in the hierarchical annealing curve are due to synthesis from one scale to the next. Immediately after synthesis, local configurations are at a high energy due to the pixels to be visited in random configurations. Since these high energies are due to local errors or inconsistencies, they are remedied easily, and energy levels immediately drop as the sampling algorithm progresses. Several different cooling schedules for the hierarchical annealing are shown in Fig. 13(b). It shows that all the reconstructions are completed in a short time and their final energies are in the same level, which illustrates that these cooling schedules are slow enough for the reconstruction system. Both Figs. 13(a) and 13(b) are presented with log-log scales. However, none of the SA results are able to match the results of HSA for both computational time and final energy.

In order to illustrate that the reconstructions quantitatively are successful, we will seek to measure and to compare their effective properties. The permeability K, which reflects some level of connectedness information about the pore space, is chosen as the effective property. Here we use pore network modeling to calculate the permeability K of the porous medium. In pore network modeling, the void space of the porous medium is represented first at the microscopic scale by a lattice of pores connected by throats [28,29]. Then, Darcy's law is applied on the pore network to calculate the permeability K of the porous medium,

$$K = \frac{Q\mu L}{A\,\Delta P}, \tag{20}$$

where A is the cross-sectional area of the domain, L is the length, and μ is the fluid viscosity. Q and ΔP are the flow rate and the pressure drop, respectively, when we specify a constant pressure drop across the network. Table I compares the permeability of the reference 3D microstructure to those of the reconstructions. It can be seen that the permeabilities of the reconstructions have similar values to that of the reference sandstone. But the permeability of the reconstructions is lower than that of the actual sandstone, which indicates that the reconstructed structures have, in general, a lower degree of

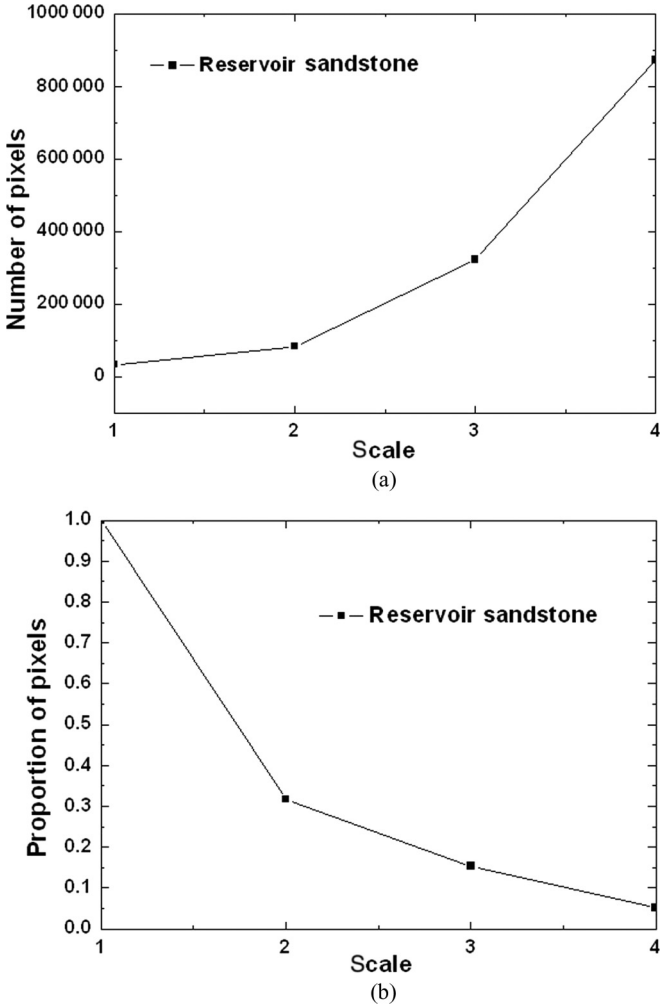

FIG. 12. The number and the proportion of pixels to be visited in a single pass of the annealer as the scale increases from $32 \times 32 \times 32$ to $256 \times 256 \times 256$.

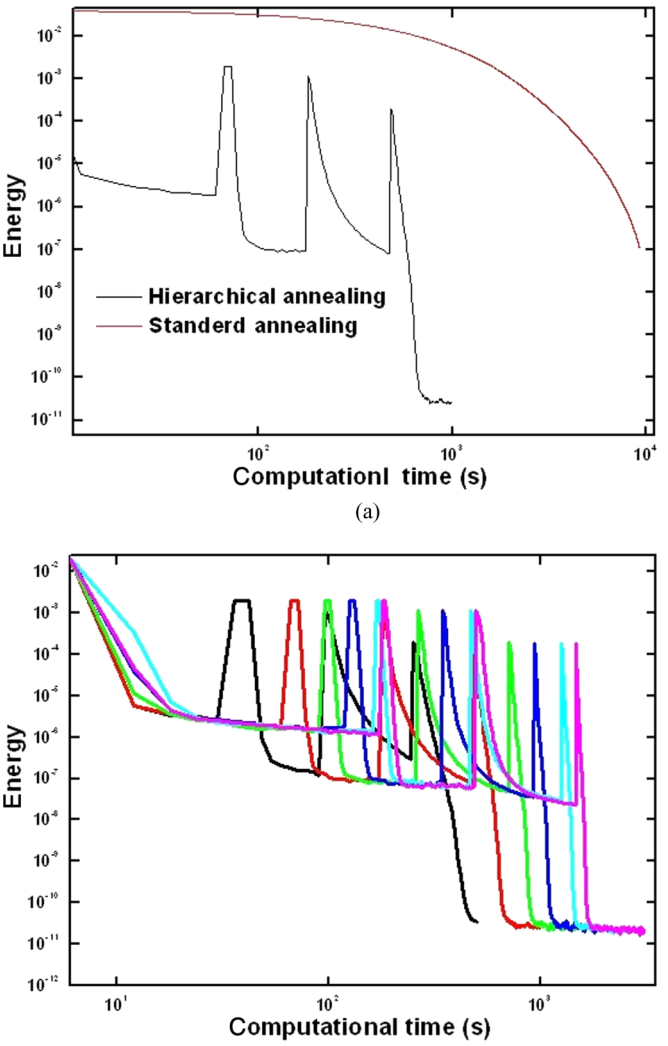

FIG. 13. (Color online) Energy vs computational time (on a 3.30 GHz Intel core i5 class machine): (a) the comparison for standard annealing and hierarchical annealing; (b) several cooling schedules for hierarchical annealing.

connectedness than that of the actual sandstone. The reason is that the two-point correlation function is not sufficient to capture full connectedness information.

V. CONCLUSION

In this paper, a stable-phase method for hierarchical annealing has been presented, which solves the high demand for computational resources associated with simulated annealing for the reconstruction of large-scale binary porous media images. In our presented method, the two-point correlation function, obtained from a 2D reference image, is used as the morphological descriptor. Because our presented method contains the reconstruction of three-phase and two-phase structures, we consider reconstructing the three-phase structures based on standard annealing and the two-phase structures based on standard and hierarchical annealings. From the result of the 2D reconstruction, we find that the reconstructions of the three-phase and two-phase structures generally capture the salient features of the reference structures. However, even though the correlation functions of the reference images and that of the generations match fairly well, the reconstructions still deviate from the reference structures. The reason is that the low-order correlation function generally does not contain complete morphological information. For the reconstructed 3D microstructure, we calculate its permeability and compare it to that of the real sandstone. The result indicates that the reconstructed microstructure cannot capture the full connectedness of the actual sandstone. The reason is that the lower-order correlation function cannot

TABLE I. The permeability of the reference and the reconstructed sandstone.

Structure	The volume fraction (ϕ_1)	Permeability (K) (mD)
Reference sandstone	0.169	3010.3
SA reconstruction	0.168	2218.8
HSA reconstruction	0.168	2101.6

capture full connectedness information. To obtain the more accurate microstructure, higher-order information should be incorporated, which will be discussed in the next paper.

The most significant advantage of our presented model is the reduction in the number of exchanged pixels by the annealer in the overall hierarchy. This paper presents the results of the reduction experienced for the generations of 3D microstructures. Only 5.21% of the pixels in the overall hierarchy need to be considered for sampling by the annealer: an order of magnitude reduction in the computational requirements. And the assertion that black and white never change at finer scales prevents large structures created at coarse scales from eroding when annealed at finer scales at high temperatures. These are the reasons that our presented method of orders of magnitude improves the convergence rate and the final energy.

ACKNOWLEDGMENTS

The authors would like to acknowledge J. H. Dunsmuir of ExxonMobil Research and Engineering Co. for providing sandstone tomograms. This work was supported by the National Natural Science Foundation of China, Grants No. 61372174 and No. 60972130.

[1] O. Melnik, Bull. Volcanol. (Heidelberg) **62**, 153 (2000).
[2] J. Høst-Madsen and K. Høgh Jensen, J. Hydrol. **135**, 13 (1992).
[3] O. Anwar Bég, R. Bhargava, S. Rawat, K. Halim, and H. S. Takhar, Meccanica **43**, 391 (2008).
[4] B. Moore, T. Jaglinski, D. Stone, and R. Lakes, Cell. Polym. **26**, 1 (2007).
[5] G. W. Scherer, Mater. Struct. **39**, 1041 (2006).
[6] N. Koshiba, J. Ando, X. Chen, and T. Hisada, J. Biomech. Eng. **129**, 374 (2007).
[7] A. M. Kraynik, Annu. Rev. Fluid Mech. **20**, 325 (1988).
[8] L. Nicolais, E. Drioli, and R. F. Landel, Polymer **14**, 21 (1973).
[9] A. I. Abdel-Hadi, O. I. Zhupanska, and N. D. Cristescu, Mech. Mater. **34**, 373 (2002).
[10] A. Belvin, R. Burrella, A. Gokhaleb, N. Thadhani, and H. Garmestani, Mater. Charact. **60**, 1055 (2009).
[11] M. Teubner, Europhys. Lett. **14**, 403 (1991).
[12] A. P. Roberts and M. A. Knackstedt, Phys. Rev. E **54**, 2313 (1996).
[13] J. F. Thovert, F. Yousefian, P. Spanne, C. G. Jacquin, and P. M. Adler, Phys. Rev. E **63**, 061307 (2001).
[14] Y. Jiao, F. H. Stillinger, and S. Torquato, Phys. Rev. E **77**, 031135 (2008).
[15] Y. Jiao, F. H. Stillinger, and S. Torquato, Proc. Natl. Acad. Sci. U.S.A. **106**, 17634 (2009).
[16] M. A. Davis, S. D. C. Walsh, and M. O. Saar, Phys. Rev. E **83**, 026706 (2011).
[17] C. E. Zachary and S. Torquato, Phys. Rev. E **84**, 056102 (2011).
[18] C. J. Gommes, Y. Jiao, and S. Torquato, Phys. Rev. Lett. **108**, 080601 (2012).
[19] C. J. Gommes, Y. Jiao, and S. Torquato, Phys. Rev. E **85**, 051140 (2012).
[20] Y. Jiao, F. H. Stillinger, and S. Torquato, Phys. Rev. E **81**, 011105 (2010).
[21] Y. Jiao, F. H. Stillinger, and S. Torquato, Phys. Rev. E **82**, 011106 (2010).
[22] M. D. Rintoul and S. Torquato, J. Colloid Interface Sci. **186**, 467 (1997).
[23] T. Tang, Q. Z. Teng, X. H. He, and D. S. Luo, J. Microsc. **234**, 262 (2009).
[24] S. K. Alexander, P. Fieguth, M. A. Ioannidis, and E. R. Vrscay, Math Geosci, **41**, 357 (2009).
[25] S. K. Alexander, P. Fieguth, and E. R. Vrscay, *Fourth International Workshop on Energy Minimization Methods in Computer Vision and Pattern Recognition*, Lecture Notes in Computer Science Vol. 2683 (Springer, Berlin, 2003), pp. 194–210.
[26] S. K. Alexander, P. Fieguth, and E. R. Vrscay, *International Conference on Image Analysis and Recognition*, Lecture Notes in Computer Science Vol. 2683 (Springer, Berlin, 2004), p. 236.
[27] S. Torquato, *Random Heterogeneous Materials* (Springer, New York, 2002).
[28] R. I. Al-Raoush and C. S. Willson, J. Hydrol. **300**, 44 (2005).
[29] A. S. Al-Kharusi and M. J. Blunt, J. Pet. Sci. Eng. **56**, 219 (2007).